IAC-13-C1.8.3

AGILE SOLAR SAILING IN THREE-BODY PROBLEM: MOTION BETWEEN ARTIFICIAL EQUILIBRIUM POINTS

Jeannette Heiligers
Advanced Space Concepts Laboratory, University of Strathclyde, U.K., jeannette.heiligers@strath.ac.uk

Colin R. McInnes
Advanced Space Concepts Laboratory, University of Strathclyde, U.K., colin.mcinnes@strath.ac.uk

This paper proposes a range of time-optimal, solar sail trajectories between artificial equilibria in the Sun-Earth three body system to create an agile solar sailing mission. This allows different mission objectives to be fulfilled at different AEPs during different stages of the mission. The analyses start from a solar sail at the sub-L_1 point (sunward of the classical L_1 point) which is targeted by NASA's Sunjammer mission (launch in 2014) for advanced space weather warning. From this sub-L_1 point, trajectories are investigated that: 1) take the solar sail to an AEP in the ecliptic plane, but slightly trailing the Earth to be ahead of the Earth in the Parker spiral to potentially increase space weather warning times even further; 2) take the solar sail to and between AEPs displaced above or below the ecliptic plane for high-latitude observations; 3) take the solar sail from the vicinity of the L_1 point to the vicinity of the L_2 point for additional Earth observations, geomagnetic tail investigations and astronomical observations. To find time-optimal trajectories, the optimal control problem associated with each of the transfers is defined and solved using a direct pseudospectral method. The resulting time of flights are reasonable, ranging from 85 days to 232 days, and the transfers are very smooth, requiring only a minimum solar sail steering effort in most cases. Since all results are generated for a sail performance equal to that of the Sunjammer sail, the proposed trajectories provide interesting end-of-mission opportunities for the Sunjammer sail after it retires at the sub-L_1 point.

I. INTRODUCTION

It is well-known that the circular restricted three-body problem (CR3BP) yields five equilibrium solutions, or Lagrange points: three along the axis connecting the two primary bodies (L_1 to L_3) and two on the remaining corners of planar equilateral triangles that connect the two primary bodies (L_4 and L_5). Adding a propulsive thrust force to the CR3BP complements these five Lagrange points with an infinite set of artificial equilibrium points (AEPs). The accessibility of these AEPs is only limited by the available propulsive acceleration, which in this paper is assumed to be provided by a solar sail.

With advances in solar sail technology through JAXA's successful IKAROS mission[1] and NASA's NanoSail-D2 mission[2] and with more solar sail missions scheduled for the next few years, including NASA's Sunjammer mission[3] and The Planetary Society's LightSail mission,[4] solar sail technology is gaining momentum. And in this paper, the use of a solar sail is proposed to exploit the wealth of AEPs available.

In the literature, as well as in real mission concepts, usually only one specific AEP is targeted for the duration of the mission, for example the Sun-Earth sub-L_1 point which lies along the Sun-Earth line, sunward of the classical L_1 point. This vantage point is ideal for achieving increased warning times for space weather events, which are currently being monitored by the ACE satellite[5] at the L_1 point. Because of its potential for advanced space weather warning, the sub-L_1 point will be targeted by NASA's Sunjammer mission, scheduled for launch in 2014. However, there is no reason why a solar sail wouldn't be able to visit multiple AEPs during a single mission, except for the time it takes to move from one AEP to the other. This paper investigates such an agile solar sail platform that allows for different mission objectives to be fulfilled at different AEPs during different parts of the mission.

The overall objective is to minimise the time-of-flight required to move between these AEPs, requiring the solution to an optimal control problem. This paper defines this optimal control problem for each transfer considered and finds solutions using a direct pseudospectral method. Results are provided for a solar sail performance equal to that of the Sunjammer solar sail. As such, it makes the proposed trajectories realistic in the near-term but also provides interesting opportunities for end-of-mission concepts once the Sunjammer sail retires at the sub-L_1 point. This would allow to demonstrate a range of solar sail applications proposed in the literature. [6-8]

With the sub-L_1 point as final destination in mind, as well as the concepts proposed in the literature, a set of transfers between a range of AEPs that are of particular interest will be considered. First, a transfer from the sub-L_1 point to an AEP in the Earth's orbital plane but trailing the Earth is considered for a potential further increase in the warning time for space weather events.

Alternatively, the sail could move from the sub-L_1 point to an AEP above the ecliptic. From such a vantage point, high-altitude telecommunications and observations of the Earth are enabled. In addition, to observe both the Earth's northern and southern hemispheres, transfers between AEPs located above and below the ecliptic plane are generated. Finally, transfers between AEPs associated with the L_1 region and those associated with the L_2 region are considered, where the AEPs close to the L_2 point provide an ideal viewpoint for astronomy as well as Earth observation and geomagnetic tail investigations.

In will be clear that, through the design of these transfers, an agile solar sail concept is created, extending a static solar sail mission to a dynamic, multi-objective mission, combining a range of potential applications including space weather, polar imaging and deep space observations.

To demonstrate the potential of these transfers, the paper will start by introducing the Sunjammer mission and its solar sail performance. Subsequently, the AEPs accessible by the Sunjammer sail are evaluated (including the sub-L_1 point) and the ones targeted in this paper are selected. Then, the transfers required to reach each of these AEPs are investigated by defining the optimal control problem, solving it and providing the results. Finally, the paper ends with the conclusions.

II. SUNJAMMER MISSION AND PERFORMANCE

NASA's Solar Sail Technology Demonstration Mission (TDM), "Sunjammer", is led by industry manufacturer L'Garde Inc. of Tustin, California, and includes participation by the National Oceanic and Atmospheric Administration (NOAA). Its aim is to demonstrate the propellantless propulsion potential of solar sails and to boost the Technology Readiness Level (TRL) of the L'Garde solar sail from ~6 to ~9. It will build on successful ground-deployment experiments led by L'Garde in 2005-2006 and the successful in-space deployment of the NanoSail-D2 mission in 2011.[*,†]

The Sunjammer solar sail will be 124 x 124 ft^2 in size, weigh about 70 pounds, and attached to it is a 175 pound disposable support module. It will be launched as a secondary payload on a Falcon 9 launcher in 2014 and its main objectives are:[†]

- Demonstrate segmented deployment of a solar sail with ~4 times the area of that vacuum tested in 2005-2006.
- Demonstrate attitude control plus passive stability and trim using beam-tip vanes.
- Execute a navigation sequence with mission-capable accuracy.
- Fly to and maintain position at L_1 (e.g. as space weather warning system) and pole sitter positions.

The characteristic acceleration of the Sunjammer solar sail is known to be in the range 0.23-0.27 mm/s^2 and is defined as:[9]

$$a_c = \beta \frac{\mu}{r_\oplus^2} \tag{1}$$

with $\mu_\odot = 1.3272 \times 10^{11}$ the gravitational parameter of the Sun and $r_\oplus = 1.4960 \times 10^8$ the Sun-Earth distance (i.e. 1 Astronomical Unit, AU). The parameter β is the solar sail lightness number, which is a function of the sail area to spacecraft mass ratio, σ, and the critical solar sail loading parameter $\sigma^* = 1.53$ g/m^2:[9]

$$\beta = \frac{\sigma^*}{\sigma} \tag{2}$$

From the range of values for the characteristic acceleration, the following range for the lightness number can be obtained:

$$\beta = 0.0388 - 0.0455 \tag{3}$$

All analyses in this paper will be executed for the extremes of this range, i.e. the minimum and maximum values, which will be referred to as case 1 ($\beta = 0.0388$) and case 2 ($\beta = 0.0455$).

III. CIRCULAR RESTRICTED THREE BODY PROBLEM

III.I Reference frame and equations of motion

In the circular restricted three body problem (CR3BP), the motion of an infinitely small mass, m, (i.e. the solar sail spacecraft), is described under the influence of the gravitational attraction of two much larger primary masses, m_1 and m_2. The gravitational influence of the small mass on the larger masses is neglected and the larger masses are assumed to move in circular orbits about their common centre-of-mass. For the Sunjammer mission, the Sun-Earth CR3BP is considered, where the Sun is represented by m_1 and the Earth by m_2. Figure 1 shows the reference frame that is employed in the CR3BP: the origin coincides with the centre-of-mass of the system, the x-axis connects the larger masses and points in the direction of the smaller of the two, m_2, while the z-axis is directed perpendicular to the plane in which the two larger masses move. The y-axis completes the right handed reference frame. Finally, the frame rotates at constant angular velocity, ω, about the z-axis, $\boldsymbol{\omega} = \omega \hat{\boldsymbol{z}}$.

[*] http://www.nasa.gov/mission_pages/tdm/solarsail/solarsail_overview.html, Retrieved 22 February 2013.

[†] http://www.lgarde.com/programs/space-propulsion/sunjammer/, Retrieved 22 February 2013.

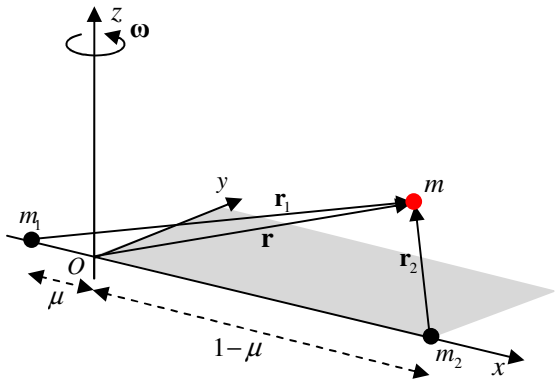

Figure 1 Schematic of circular restricted three-body problem.

New units are introduced: the sum of the two larger masses is taken as the unit of mass, i.e. $m_1 + m_2 = 1$. Then, with the mass ratio $\mu = m_2 / (m_1 + m_2)$, the masses of the large bodies become $m_1 = 1-\mu$ and $m_2 = \mu$. As unit of length, the distance between the main bodies is selected, and $1/\omega$ is chosen as unit of time, yielding $\omega = 1$, and so one year is represented by 2π.

In this reference system, the motion of the solar sail is described by:[9]

$$\ddot{\mathbf{r}} + 2\boldsymbol{\omega}\times\dot{\mathbf{r}} + \boldsymbol{\omega}\times(\boldsymbol{\omega}\times\mathbf{r}) = \mathbf{a}_s - \nabla V \tag{4}$$

with $\mathbf{r} = [x \quad y \quad z]^T$ the position vector of m. The terms on the left hand side are the kinematic, coriolis and centripetal accelerations, respectively, while the terms on the right hand side are the solar sail acceleration and the gravitational acceleration exerted by the primary masses. In the CR3BP reference frame, an ideal solar sail acceleration, as assumed in this paper, is defined as:[9]

$$\mathbf{a}_s = \beta \frac{1-\mu}{r_1^2}(\hat{\mathbf{r}}_1 \cdot \hat{\mathbf{n}})^2 \hat{\mathbf{n}} \tag{5}$$

while the gravitational potential, V, is given by:

$$V = -\left(\frac{1-\mu}{r_1} + \frac{\mu}{r_2}\right) \tag{6}$$

Note that the vectors $\mathbf{r}_1$ and $\mathbf{r}_2$ are defined as $\mathbf{r}_1 = [x+\mu \quad y \quad z]^T$ and $\mathbf{r}_2 = [x-(1-\mu) \quad y \quad z]^T$. Furthermore, due to the assumption of an ideal solar sail, the solar sail acceleration is parallel to the normal to the sail surface, $\mathbf{n}$. Finally, following Reference 9, the centripetal acceleration in Eq. (4) can be written as the gradient of a scalar potential function, $\Phi = -\frac{1}{2}\|\boldsymbol{\omega}\times\mathbf{r}\|^2$, and can be combined with the gravitational potential into a new, effective potential, U:

$$U = -\frac{x^2+y^2}{2} - \left(\frac{1-\mu}{r_1} + \frac{\mu}{r_2}\right) \tag{7}$$

The new set of equations of motion then become:

$$\ddot{\mathbf{r}} + 2\boldsymbol{\omega}\times\dot{\mathbf{r}} = \mathbf{a}_s - \nabla U \tag{8}$$

III.II Equilibrium surfaces

Equilibrium point solutions to Eq. (8) can be found by setting $\ddot{\mathbf{r}} = \dot{\mathbf{r}} = 0$. For $\mathbf{a}_s = 0$ this yields the classical five Lagrange points, while for $\mathbf{a}_s \neq 0$ additional, artificial equilibrium points (AEPs) can be found. The required solar sail acceleration to maintain an arbitrary AEP in the CR3BP is then given by:

$$\mathbf{a}_s = \nabla U \tag{9}$$

Following the analysis in Reference 9, the required direction of this solar sail acceleration as well as the required solar sail lightness number can be derived:

$$\mathbf{n} = \frac{\nabla U}{|\nabla U|} \tag{10}$$

$$\beta = \frac{r_1^2}{1-\mu}\frac{\nabla U \cdot \mathbf{n}}{(\hat{\mathbf{r}}_1 \cdot \mathbf{n})^2} \tag{11}$$

The required sail lightness number is thus only a function of the position within the CR3BP reference frame. Therefore, equilibrium surfaces can be drawn in the CR3BP reference frame for constant lightness number. These surfaces (projected as contours on the (x,y)-plane and (x,z)-plane) are provided in Figure 2.

Note that the white areas in Figure 2 indicate regions in which no equilibrium solutions exist for the solar sail as these regions would require an acceleration with a component in the direction of the Sun, which the solar sail is unable to generate.[9] Furthermore, by setting Eq. (11) equal to the lightness numbers for case 1 and 2 derived for the Sunjammer solar sail in the previous section, the equilibrium solutions presented with the white line (case 1) and grey line (case 2) can be obtained.

A three-dimensional view of the contour plots is provided in

Figure 3 for case 1 and case 2 combined, both excluding (a) and including (b-d) the 'forbidden' regions for the solar sail. Note that, when including the 'forbidden' regions, the small spherical surface to the right of the L_1-point disappears, but the small spherical surface to the left of the L_2-point remains.

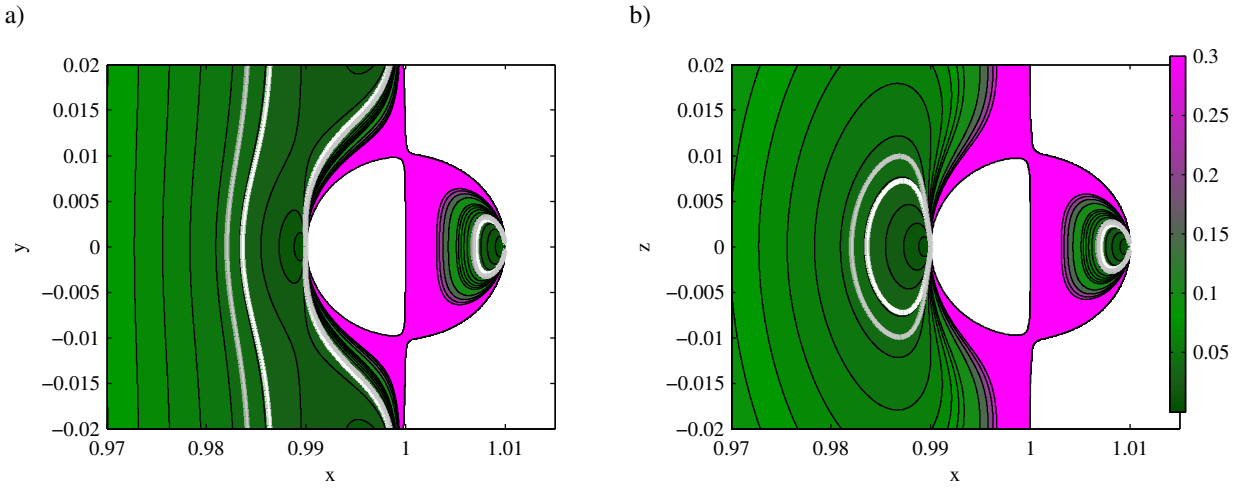

Figure 2 Projected contour plots for β =[10-8 0.01 0.02 0.03 0.04 0.05 0.06 0.07 0.08 0.09 0.1 0.15 0.2 0.25 0.3] (from dark green to pink). The white line is the contour for case 1 (β = 0.0388), while the grey line is the contour for case 2 (β = 0.0455).

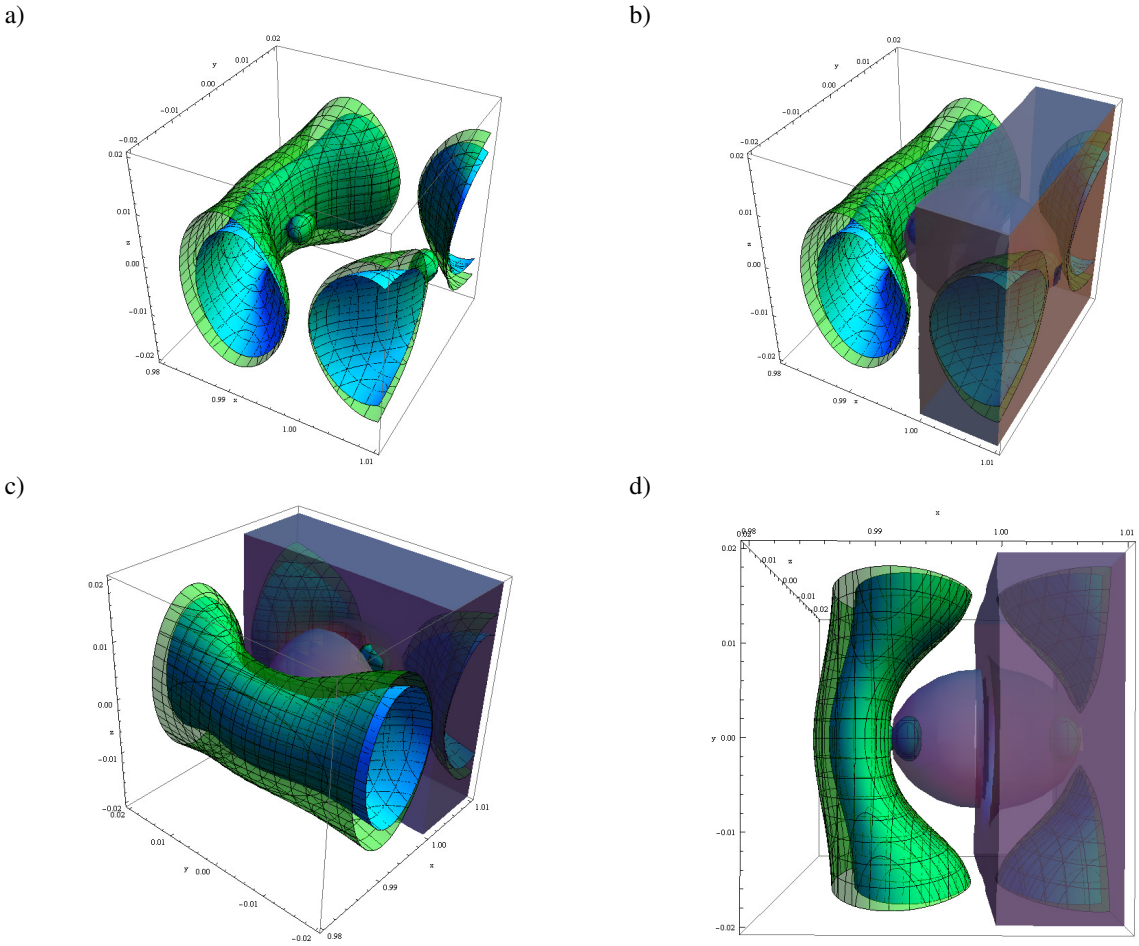

Figure 3 Combined equilibrium surfaces for cases 1 (blue/inner) and 2 (green/outer). a) Excluding and b-d) Including the solar sail 'forbidden' regions.

III.III Sub-L_1 positions

From Figure 2 and Figure 3 the sub-L_1 points corresponding to both Sunjammer sail lightness number cases can be derived by obtaining the coordinates of the locations where the contours intersect the x-axis and selecting the crossing with the smallest value for the x-coordinate (i.e. closest to the Sun). The results are provided in Table 1. Considering the fact that the classical L_1-point is located at $x = 0.99002598$ (1,491,642 km from the Earth), the Sunjammer solar sail can increase the warning time for space weather events by a factor 1.6 - 1.8 compared to the existing ACE satellite at the L_1 point. To remain at these sub-L_1 points, a solar sail acceleration parallel to the x-axis is needed, requiring the sail surface to be oriented perpendicular to the Sun-sail line.

Case	β	x-position sub-L_1 point	Distance from Earth, km	Increase in warning time
1	0.0388	0.9837	2,437,996	1.63
2	0.0455	0.9821	2,677,352	1.79

Table 1 Sub-L_1 data for cases 1 and 2.

III.IV Selected AEPs

As indicated in the introduction of the paper, a range of AEPs, other than the sub-L_1 point, will be considered for additional mission objectives compared to a pure sub-L_1 mission. The AEPs selected are depicted in Figure 4 and are listed below. Additional information on each AEP will be provided in the next subsections that deal with each AEP and each transfer separately:

- Red dots: AEPs in the ecliptic plane trailing the Earth at an angle of 45 deg. This AEP is selected as it is ahead of the Earth in the Parker spiral and as such can potentially increase the space weather warning time even further.
- Blue crosses: The AEP with the maximum achievable out-of-plane displacement *above* the ecliptic, which can enable high-latitude telecommunications and Earth observations. [6, 10]
- Green squares (coinciding with the blue squares in the (x, y)-plane in Figure 4a): The AEP with the maximum achievable out-of-plane displacement *below* the ecliptic, which can serve the same purpose as the blue cross-AEPs but than for the southern hemisphere.
- Yellow stars: The AEP on the equilibrium surface associated with the L_2 point, in the ecliptic plane and with the minimum distance to Earth. From this AEP, Earth observations as well as astronomical observations and geomagnetic tail investigations can be performed.

From Figure 4, the advantage of the larger lightness number of case 2 becomes clear: not only will it allow a larger warning time for space weather events as the sub-L_1 point for case 2 is located closer to the Sun and further ahead in the Parker spiral, but it also allows for the largest out-of-ecliptic displacement (i.e. hovering above higher Earth latitudes) and it is closer to the Earth at the AEP in the L_2-region, which is advantageous for Earth observation purposes.

Transfers to and between these AEPs will be considered in the next section and subsections.

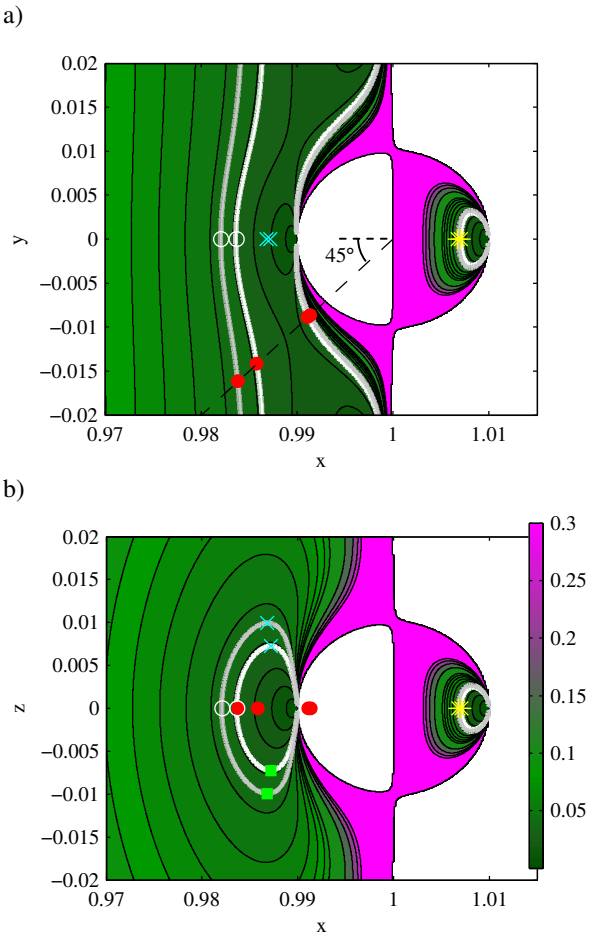

Figure 4 Selected AEPs.

IV. MOTION BETWEEN EQUILIBRIOUM POINTS

Before starting the discussion on the design of the transfers, it is noted that, although degradation of the solar sail will eventually have to be taken into account, no such data is currently available for the Sunjammer solar sail. Therefore, for the results presented in this

section, the lightness number is assumed to be equal to the lightness numbers at the start of the mission, i.e. as calculated in Section II.

IV.I Optimal control problem

As stated in the introduction, the objective is to find time-optimal trajectories between the AEPs selected in Section III.IV. In order to do so, the accompanying optimal control problem needs to be solved. This is done using the software package PSOPT.[11] PSOPT is an open source tool developed by Victor M. Becerra of the University of Reading, UK, which is a particular implementation of a direct pseudospectral method in C++. It can use both Legendre and Chebyshev polynomials to approximate and interpolate the dependent variables at the nodes and has interfaces to two NLP solvers: IPOPT (Interior Point OPTimizer), an open source C++ implementation of an interior point method for large scale problems, see Reference [12], and SNOPT (Sparse Nonlinear OPTimizer), a well-known and widely used proprietary large scale NLP solver, see Reference [13]. However, in this work only the Legendre pseudospectral method and IPOPT have been used.

Since the optimal control problem is very similar for each of the transfers defined in Section III.IV, this section provides an outline of the general optimal control problem to be solved. Problem specific information (i.e. the event constraints) will then be provided further on, in the subsections dealing with each particular transfer.

The optimal control problem can be defined as: finding the state history, $\mathbf{x}(t)$, and control history, $\mathbf{u}(t)$, that minimises the cost function:

$$J = t_f - t_0 \tag{12}$$

The state and control vectors, $\mathbf{x}(t)$ and $\mathbf{u}(t)$, are composed of the following state and control variables:

$$\mathbf{x} = \begin{bmatrix} x & y & z & \dot{x} & \dot{y} & \dot{z} \end{bmatrix}^T \tag{13}$$

$$\mathbf{u} = \begin{bmatrix} n_x & n_y & n_z \end{bmatrix}^T \tag{14}$$

with x, y, z, $\dot{x}$, $\dot{y}$ and $\dot{z}$ the position and velocity components in the CR3BP reference frame and n_x, n_y and n_z the Cartesian components of the solar sail normal vector in the CR3BP reference frame.

While minimising the objective function in Eq. (12), the dynamics of the system have to be satisfied (i.e. Eq. (4)) as well as a set of constraints, including path constraints, event constraints and bounds on the states, controls and time. The path constraints include:

$$|\mathbf{n}| = 1 \tag{15}$$

$$(\hat{\mathbf{r}}_1 \cdot \mathbf{n}) \geq 0 \tag{16}$$

where the first path constraint ensures that the norm of the solar sail normal vector equals unity and the second path constraint prevents the use of a solar sail component in the direction of the Sun, which the solar sail is unable to generate.

As indicated before, the event constraints on the initial and final state vectors, $\mathbf{x}_0$ and $\mathbf{x}_f$, are problem specific as they are equal to the state vector at the start and end of the trajectory, which will coincide with either the sub-L_1 point or any of the AEPs selected in Section III.IV. The actual values will be given in the respective subsection.

Finally, to solve the optimal control problem, PSOPT requires a suitable initial guess. Where possible, the initial guess trajectory follows the contours of the equilibrium surfaces. Furthermore, the control vector along the initial guess trajectory is assumed to be the sail normal vector as if each point along this trajectory were an instantaneous AEP, i.e. the control vector is given by Eq. (10). In general, such an initial guess allowed for a smooth optimisation process and quick convergence to the optimal solution.

IV.II Sub L_1 to AEP ahead in Parker spiral

In addition to studies to place a spacecraft at a sub-L_1 point for increased space weather warning times, some studies propose to use solar wind measurements in an Earth trailing orbit (e.g. the L_5 point) for the same purpose and claim to achieve even greater warning times.[14, 15] The reason being that, while trailing the Earth in its orbit, the spacecraft or solar sail would be ahead of the Earth in the Parker spiral: due to its rotation, the Sun's magnetic field extends into the solar system through an Archimedean spiral, called the Parker spiral. The solar wind travels along this spiralling motion, thereby sweeping by the L_5 point first before arriving at Earth. Based on this, an increase in the space weather warning time could be achieved if the solar sail would be trailing the Earth.

According to this principle, an AEP is selected on the Sunjammer sail equilibrium surfaces that is located in the ecliptic plane, but trailing the Earth by an angle of 45 deg, see the red dots and black dashed line in Figure 4a. It must be noted that the value of 45 deg is selected at random and serves as an example since very similar trajectories could be generated for any other value for this angle. Furthermore, it is clear that the black dashed line crosses the equilibrium surfaces twice, once on the Sun-side of the surface and once on the Earth-side. Both AEPs will be considered in this section and the corresponding coordinates are given in Table 2 for both case 1 ($\beta = 0.0388$) and case 2 ($\beta = 0.0455$).

In order to transfer from the sub-L_1 point to the AEPs specified in Table 2, the optimal control problem defined in Section IV.I needs to be solved with the following event constraints on $\mathbf{x}_0$ and $\mathbf{x}_f$:

$$\mathbf{x}_0 = \mathbf{x}_{\text{sub-L}_1} \tag{17}$$

$$\mathbf{x}_f = \begin{bmatrix} x_{45\,\text{deg}} & y_{45\,\text{deg}} & 0 & 0 & 0 & 0 \end{bmatrix}^T \tag{18}$$

with $\mathbf{x}_{\text{sub-L}_1}$ the state vector at the sub-L_1 point, see Table 1.

Hereafter, first the transfer from sub-L_1 to the Sun-side 45 deg AEP will be considered, followed by the transfer from sub-L_1 to the Earth-side 45 deg AEP.

	$x_{45\,\text{deg}}$	$y_{45\,\text{deg}}$	$z_{45\,\text{deg}}$
AEP on Sun-side of equilibrium surface			
Case 1	0.98581	-0.01416	0
Case 2	0.98381	-0.01608	0
AEP on Earth-side of equilibrium surface			
Case 1	0.99112	-0.00888	0
Case 2	0.99135	-0.00864	0

Table 2 Coordinates of 45 deg Earth trailing AEPs.

IV.II.i Sub L_1 to Sun-side 45 deg AEP

The initial guess for the transfer to the Sun-side 45 deg AEP is provided in Figure 5 and complies with the description in Section IV.I: the initial guess follows the contour (and therefore lies entirely in the (x, y)-plane) and the control law equals the normal vector of the solar sail as if each point along this trajectory were an instantaneous AEP. Furthermore, a transfer time of half a year is assumed.

The result of solving the optimal control problem is shown in Figure 6 for cases 1 (plot a) and 2 (plot b). Again, the trajectory lies entirely in the (x, y)-plane, so plots of the trajectory in the (x, z)-plane are omitted. Both trajectories require a very smooth control law as indicated by the arrows that represent the solar sail normal vector and take 227 and 223 days, respectively, to complete, see Table 3. This indicates that, despite the longer trajectory (in terms of arc length) for case 2, the larger sail lightness number allows a shorter transfer time.

IV.II.ii Sub L_1 to Earth-side 45 deg AEP

A very similar approach can be taken for the transfer to the Earth-side 45 deg AEP. The main difference is the initial guess, which is now assumed to be a straight line connecting the initial and final state-vectors in the ecliptic plane, but still assuming that the control vector is the normal vector of the solar sail as if each point along the trajectory were an instantaneous AEP. Again, a transfer time of half a year is assumed. This initial guess is shown in Figure 7, while the optimised trajectories are given in Figure 8. Again, the entire trajectory lies in the (x, y)-plane only.

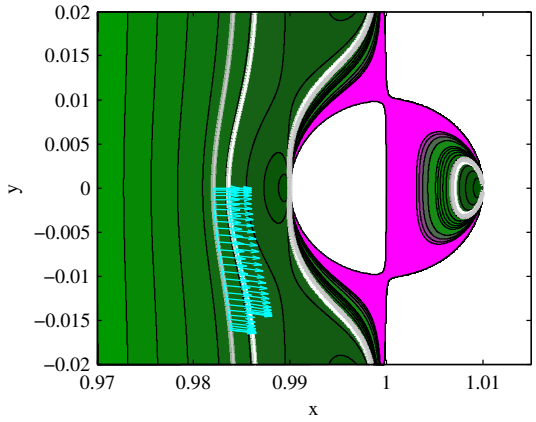

Figure 5 Initial guess in (x,y)-plane for transfer from sub-L_1 point to Sun-side 45 deg AEP.

a)

b)

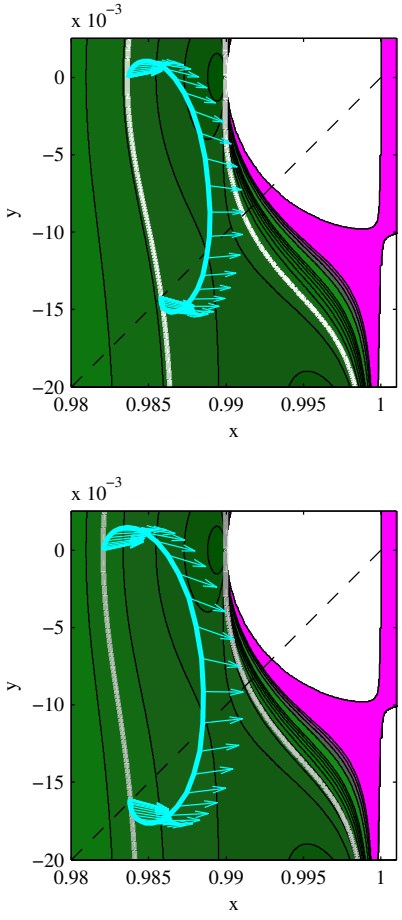

Figure 6 Optimal transfers from sub-L_1 to Sun-side 45 deg AEP with arrows indicating the solar sail normal vector. a) Case 1. b) Case 2.

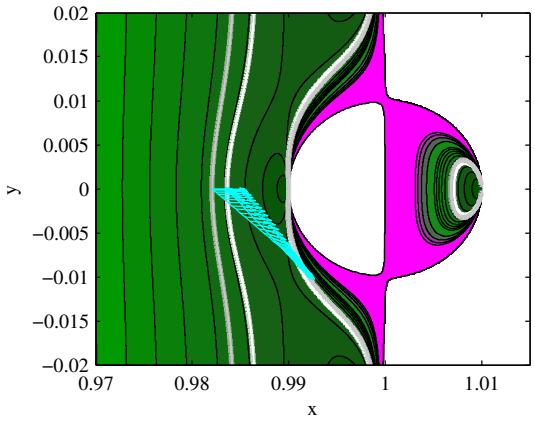

Figure 7 Initial guess in (x,y)-plane for transfer from sub-L_1 point to Earth-side 45 deg AEP.

a)

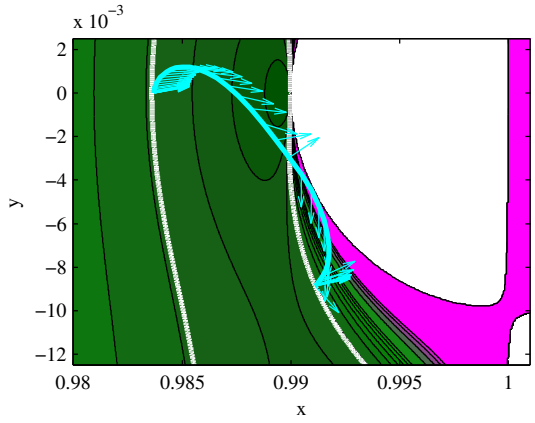

b)

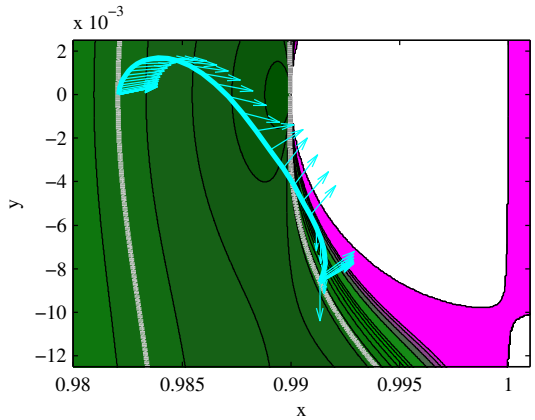

Figure 8 Optimal transfers from sub-L_1 to Earth-side 45 deg AEP with arrows indicating the solar sail normal vector. a) Case 1. b) Case 2.

	Time of flight, days
AEP on Sun-side of equilibrium surface	
Case 1	227
Case 2	223
AEP on Earth-side of equilibrium surface	
Case 1	133
Case 2	132

Table 3 Minimum time of flights for sub-L_1 to 45 deg AEPs transfers.

Although the control seems to be less smooth than for the trajectories in Figure 6, the only irregularity is a period of ballistic flight when the normal vector is pointed perpendicular to the Sun-sail line. The minimum time of flights are added to Table 3 and show that 133 to 132 days are required to perform the transfer. Again, the larger lightness number for case 2 outweighs the longer arc length, allowing a slightly shorter transfer time than for case 1.

IV.III Sub-L_1 to maximum out-of-ecliptic AEP transfer

The second transfer to be considered enables a demonstration of maintaining an artificial equilibrium point displaced away from the ecliptic plane. It aims for the maximum achievable out-of-plane displacement *above* the ecliptic, see the blue crosses in Figure 4, to enable high-latitude Earth observation and communications. The coordinates of this maximum out-of-ecliptic AEP are provided in Table 4. These correspond to a spacecraft-Earth-Sun angle (i.e. the latitude above which the satellite would hover if the polar axis of the Earth is assumed parallel to the z-axis) of 29.5° and 37.0° for cases 1 and 2, respectively.

Again assuming the sub-L_1 point as starting point and using the coordinates in Table 4, the following event constraints can be defined:

$$\mathbf{x}_0 = \mathbf{x}_{\text{sub-L}_1} \tag{19}$$

$$\mathbf{x}_f = \mathbf{x}_{z_{\max}} \tag{20}$$

with $\mathbf{x}_{z_{\max}}$ the state-vector at the maximum out-of-ecliptic AEP:

$$\mathbf{x}_{z_{\max}} = \begin{bmatrix} x_{z_{\max}} & 0 & z_{\max} & 0 & 0 & 0 \end{bmatrix}^T \tag{21}$$

	$x_{z_{\max}}$	$y_{z_{\max}}$	$z_{\max}$
Case 1	0.98719	0	0.0072398
Case 2	0.98683	0	0.0099383

Table 4 Coordinates of maximum out-of-ecliptic AEPs.

To generate the initial guess the same approach as for the sub-L_1 to Sun-side 45 deg AEP is taken, see Figure 9. These initial guesses are assumed to take half a year and lie in the (x,z)-plane only, contrary to the optimised transfers shown in Figure 10.

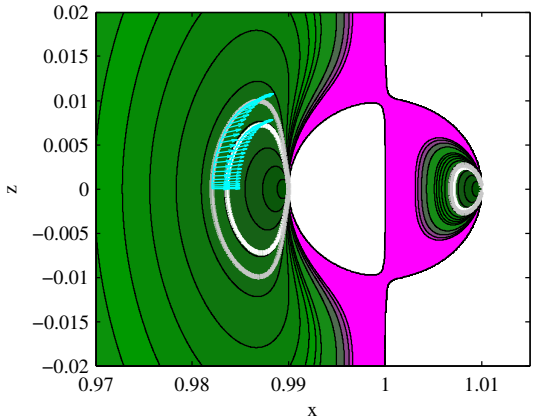

Figure 9 Initial guess in (x,z)-plane for transfer from sub-L_1 point to maximum out-of-ecliptic AEP.

While plots a-b show the results for case 1, plots c-d show the results for case 2. The arrows again indicate a very smooth control that requires a minimum steering effort from the solar sail. Finally, the minimised time of flights shown in Table 5 show relatively quick transfers of approximately 100 days. This time, the larger sail lightness number of case 2 cannot compensate for the longer trajectory arc, resulting in a slightly longer transfer time for case 2 than for case 1.

	Time of flight, days
Case 1	106
Case 2	114

Table 5 Minimum time of flights for sub-L_1 to maximum out-of-ecliptic AEPs transfers.

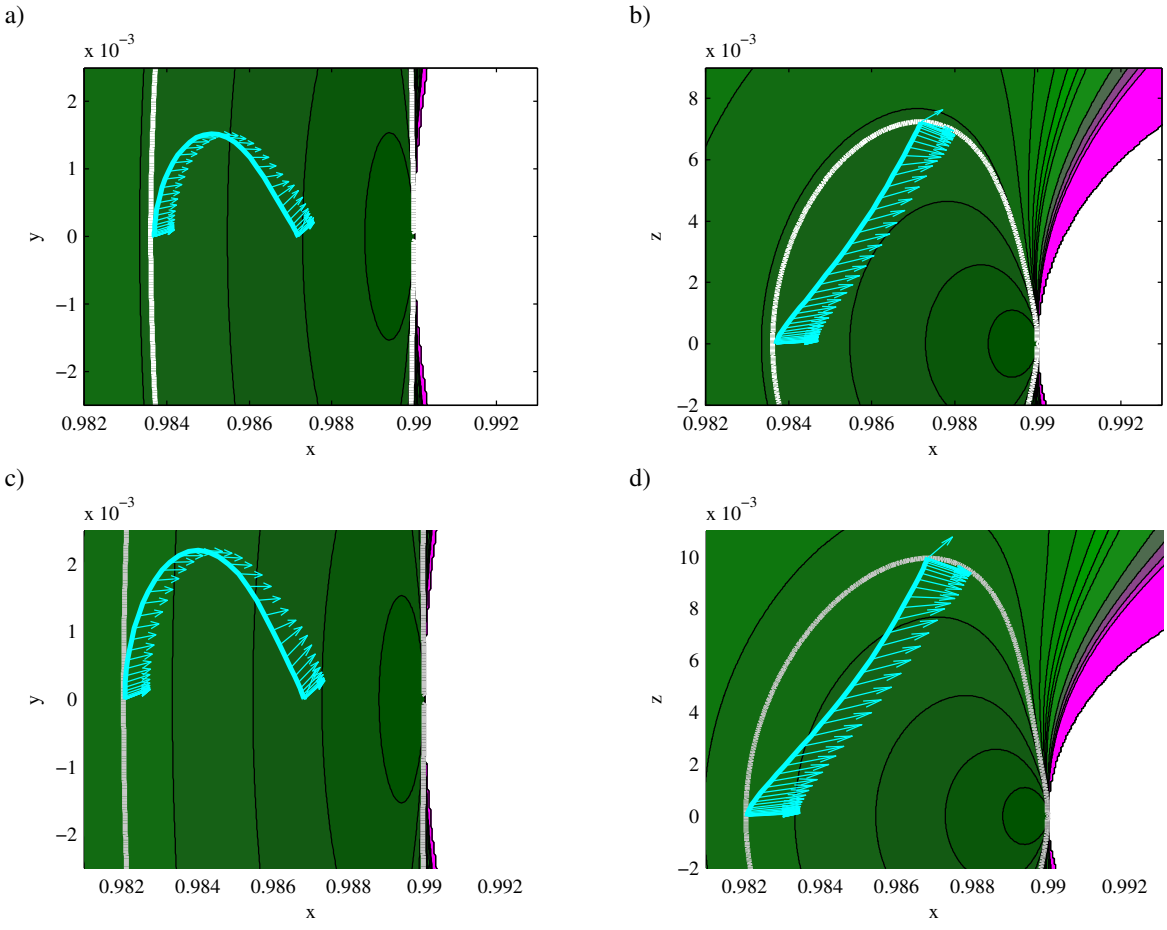

Figure 10 Optimal transfers from sub-L_1 to the maximum out-of-ecliptic AEP with arrows indicating the solar sail normal vector. a-b) Case 1. c-d) Case 2.

IV.IV North to south elevated AEPs

While section IV.III only considered the maximum out-of-plane AEP *above* the ecliptic ('north'), this section will also exploit the AEP with the maximum out-of-plane displacement *below* the ecliptic ('south'), see the green squares in Figure 4b (which coincide with the blue crosses in Figure 4a). The idea being that transferring from north-to-south demonstrates the possibility of observing both the northern and southern hemispheres of the Earth from outside the ecliptic with a single platform.

Clearly, due to symmetry, the coordinates for the south AEP will be equal to those for the north AEP, see Table 4, only mirroring the z-coordinate in the ecliptic plane. The boundary conditions for a transfer from north-to-south then become:

$$\mathbf{x}_0 = \mathbf{x}_{z^+_{\max}} \tag{22}$$

$$\mathbf{x}_f = \mathbf{x}_{z^-_{\max}} \tag{23}$$

with

$$\mathbf{x}_{z^+_{\max}} = \begin{bmatrix} x_{z_{\max}} & 0 & z_{\max} & 0 & 0 & 0 \end{bmatrix}^T \tag{24}$$

$$\mathbf{x}_{z^-_{\max}} = \begin{bmatrix} x_{z_{\max}} & 0 & -z_{\max} & 0 & 0 & 0 \end{bmatrix}^T \tag{25}$$

The initial guess for the optimal control problem assumes a straight line in the (x,z)-plane between the initial and final conditions, see Figure 11, similar to the transfer in Figure 7, and is assumed to take half a year. Furthermore, as has been the case for every transfer so far, the initial guess for the control vector along this trajectory is the sail normal vector required as if each position along the initial guess were an AEP.

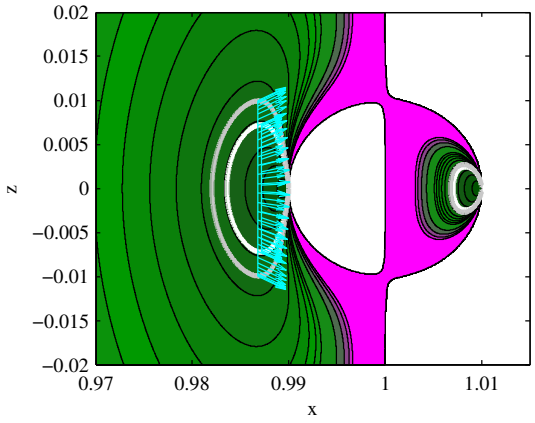

Figure 11 Initial guess for north-to-south elevated AEPs transfer.

The results for both lightness number cases are provided in Figure 12 and Figure 13, respectively. Note the difference in scale between the (x,y)- and (x,z)-projections, indicating only a very subtle motion in the ecliptic plane during the transfer. From the optimal transfer times in Table 6 it furthermore becomes clear that the required transfer time is approximately a quarter of a year, which would be quick enough to observe the northern and southern hemispheres during their respective summers. Again, despite the larger sail lightness number, the longer transfer arc causes the transfer time for case 2 to be longer than for case 1.

	Time of flight, days
Case 1	85
Case 2	91

Table 6 Minimum time of flights for north-to-south elevated AEPs transfers.

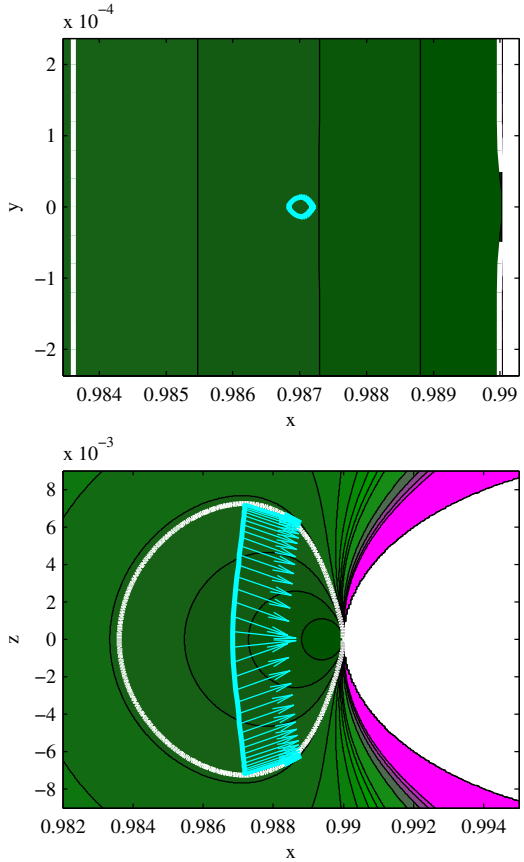

Figure 12 Case 1: optimal north-to-south elevated AEPs transfer.

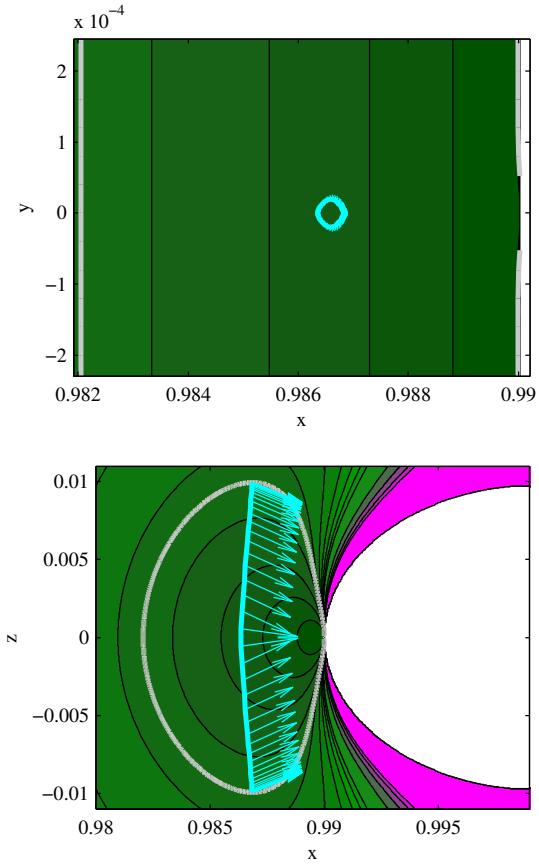

Figure 13 Case 2: optimal north-to-south elevated AEPs transfer.

IV.V L_1 to L_2 region transfer

The final type of transfer that is considered is a transfer between the contours in close vicinity of the L_1-point to the contours associated with the L_2-point. Hovering close to the L_2-point would allow for observations of the night-side of the Earth, geomagnetic tail investigations as well as astronomical observations. The point targeted along the L_2-contour lies in the ecliptic plane and is the point closest to the Earth, see the yellow stars in Figure 4 and the coordinates in Table 7. Assuming that this transfer is executed after a sequence of north-to-south transfers described in the previous section, the starting point of the transfer will be the north AEP. The event constraints then become:

$$\mathbf{x}_0 = \mathbf{x}_{z^+_{\max}} \tag{26}$$

$$\mathbf{x}_f = \mathbf{x}_{L_2} \tag{27}$$

with

$$\mathbf{x}_{L_2} = \left[x_{L_2, x_{\min}} \quad 0 \quad 0 \quad 0 \quad 0 \quad 0 \right]^T \tag{28}$$

To initiate solving the optimal control problem, the initial guess as shown in Figure 14 is used, which is now assumed to take a full year due to the significant distance which it has to traverse. Due to the approach of generating the initial guess for the control, i.e. by computing the sail normal vector as if each position along the initial guess were an AEP, the initial guess needs to circumvent the white, forbidden sail region. The initial guess therefore looks peculiar, but still allows a very smooth optimisation process and very quick convergence to the optimal solutions, which are provided in Figure 15. These optimal results show more complicated transfers than those considered in Sections IV.II to IV.IV, with periods of no (case 1) or very little (case 2) thrusting when the spacecraft is in the white, forbidden region. Furthermore, the sail passes below and 'behind' the Earth in its orbit around the Sun and seems to use this "Earth swing-by" to smoothly wind onto the L_2 associated equilibrium surface. Finally, the blue arrows indicate that the steering scheme is also more demanding than for the optimal transfers in Sections IV.II to IV.IV, but the required time of flights (see Table 8) can still be considered reasonable.

Interest hot topic

a)

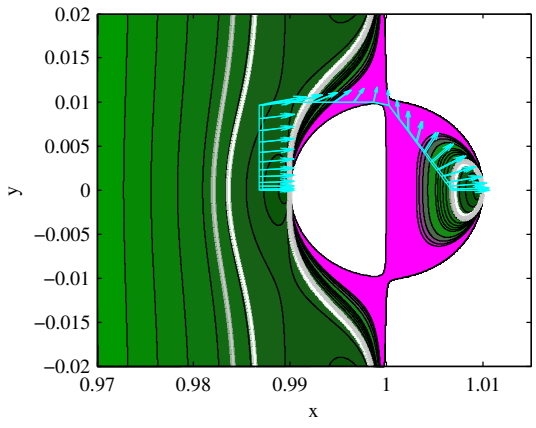

b)

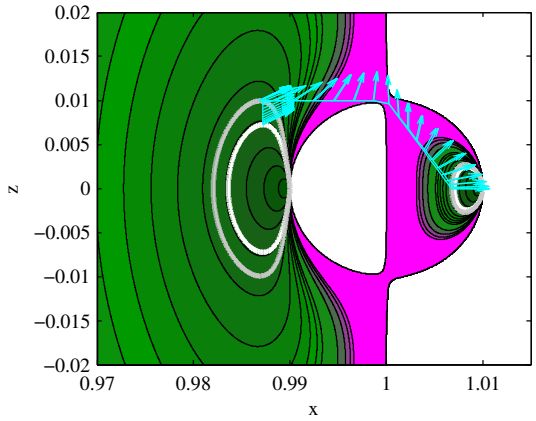

Figure 14 Initial guess for L_1-to-L_2 region transfer.

	$x_{L_2,x_{\min}}$	$y_{L_2,x_{\min}}$	$z_{L_2,x_{\min}}$
Case 1	1.0071	0	0
Case 2	1.0068	0	0

Table 7 Coordinates of L_2-region AEPs.

	Time of flight, days
Case 1	232
Case 2	223

Table 8 Minimum time of flights for L_1-to-L_2 region transfers.

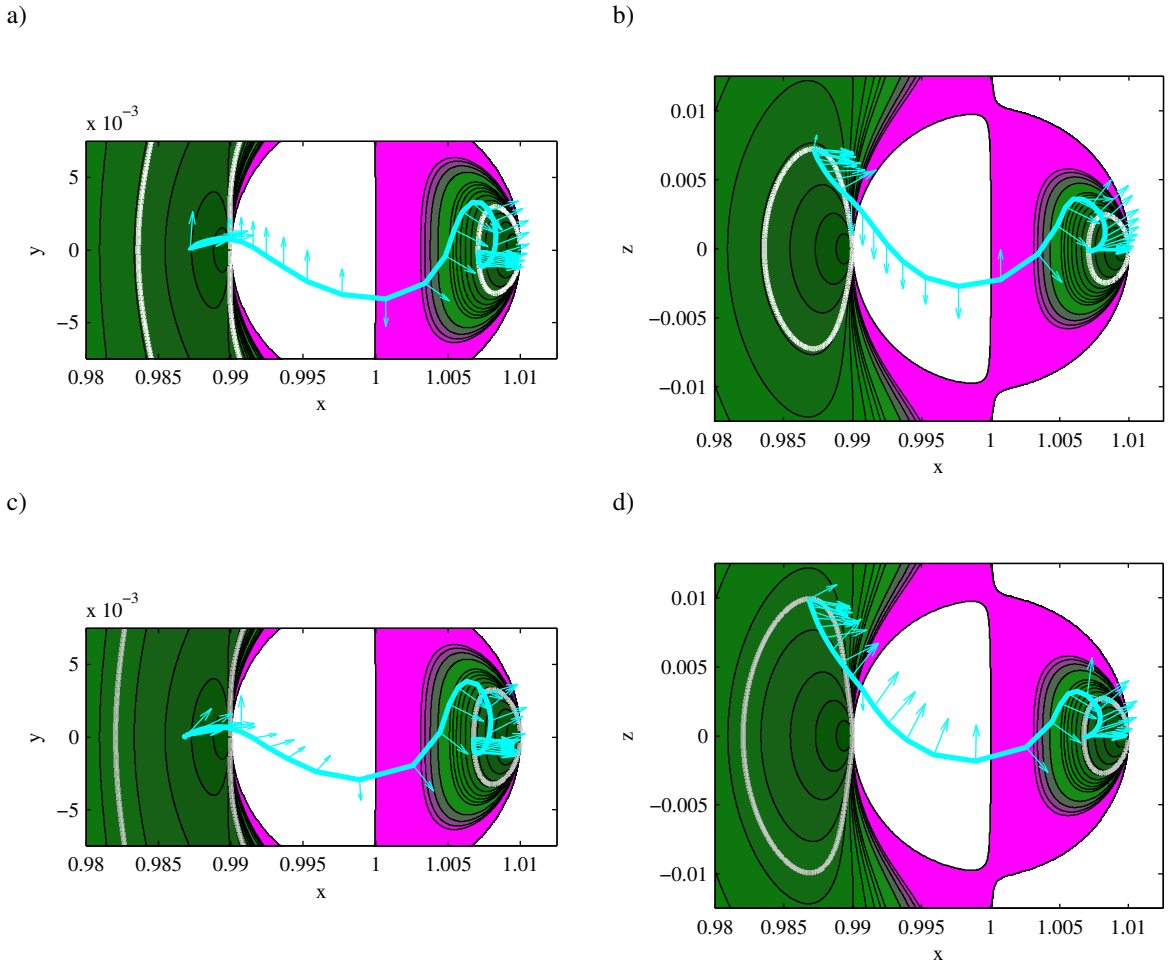

Figure 15 Optimal L_1-to-L_2 region transfers. a-b) Case 1. c-d) Case 2.

V. CONCLUSIONS

In this paper a set of transfers have been proposed that allow a tour along several artificial equilibrium points (AEPs) in the solar sail Sun-Earth three body problem, each of which can provide unique space applications. With NASA's solar sail Sunjammer mission scheduled for launch next year, all transfers are designed with the Sunjammer sail performance in mind, thereby providing interesting end-of-mission opportunities for the sail after the mission terminates at the sub-L_1 point. This paper has demonstrated that, from this sub-L_1 point, which lies along the Sun-Earth line, but Sunward of the classical L_1 point, the Sunjammer sail can achieve an increase in the warning time for space weather events by a factor 1.63 to 1.79 compared to existing hardware at the classical L_1 point.

Additionally, transfers from this sub-L_1 position to AEPs slightly trailing the Earth to be ahead in the Parker spiral have been considered which would allow an investigation whether such an AEP could increase the achievable warning time even further. Furthermore, transfers from the sub-L_1 position to AEPs high above the ecliptic have been considered as demonstration of high-latitude observations from within the three-body

problem as well as transfers from above to below the ecliptic (or from north-to-south) to observe both hemispheres of the Earth. Finally, a transfer that brings the sail from AEPs associated with the L_1 region to AEPs associated with the L_2 region have been investigated. Hovering on the night-side of the Earth would allow for Earth observation, magnetic tail investigations as well as astronomical observations.

All transfers show reasonable time of flights, ranging from a quarter of a year for the north-to-south transfer (allowing observation of the northern and southern hemispheres during their respective summers) to 232 days for the transfer from the L_1 region to the L_2 region. In all cases, two values for the lightness number have been considered in correspondence to the expected performance of the Sunjammer sail, i.e. a characteristic acceleration in the range 0.23-0.27 mm/s^2. The larger value allows the sail to be located closer to the Sun, further ahead in the Parker spiral, and farther out of the ecliptic. Despite the longer transfer arcs (in terms of length) that result from this, the larger available acceleration in some cases translates into slightly shorter transfer times than for the smaller value of the characteristic acceleration. In all cases, the transfers are very smooth and in most cases require only a minimum steering effort from the solar sail.

Future investigations will include a more detailed modelling of the solar sail acceleration, including degradation of the sail at the end of the Sunjammer mission as well as non-ideal properties of the solar sail.

ACKNOWLEDGEMENTS

This work was funded by the European Research Council Advanced Investigator Grant-227571: Visionary Space Systems: Orbital Dynamics at Extremes of Spacecraft Length-Scale.

REFERENCES

[1] Tsuda, Y., Mori, O., Funase, R., Sawada, H., Yamamoto, T., Saiki, T., Endo, T., and Kawaguchi, J. "Flight Status of IKAROS Deep Space Solar Sail Demonstrator," *Acta Astronautica* Vol. 69, No. 9-10, 2011, pp. 833-840. Doi: 10.1016/j.actaastro.2011.06.005

[2] Johnson, L., Whorton, M., Heaton, A., Pinson, R., Laue, G., and Adams, C. "NanoSail-D: A Solar Sail Demonstration Mission," *Acta Astronautica* Vol. 68, 2011, pp. 571-575. Doi: 10.1016/j.actaastro.2010.02.008

[3] L'Garde Inc. "L'Garde - Sunjammer." http://www.lgarde.com/programs/space-propulsion/sunjammer, Accessed 8 May 2013.

[4] Biddy, C., and Svitek, T. "LightSail-1 Solar Sail Design and Qualification," *Proceedings of the 41st Aerospace Mechanisms Symposium*. Pasadena, CA, 2012.

[5] Goddard Space Flight Center. "Advanced Composition Explorer ACE - Detailed Mission Requirements (Report number GSFC-410-ACE-017)." 1995.

[6] McInnes, C. R., McDonald, A. J., Simmons, J. F. L., and MacDonald, E. W. "Solar Sail Parking in Restricted Three-Body Systems," *Journal of Guidance, Control, and Dynamics* Vol. 17, No. 2, 1994, pp. 399-406. Doi: 10.2514/3.21211

[7] Waters, T. J., and McInnes, C. R. "Periodic Orbits Above the Ecliptic in the Solar-Sail Restricted Three-Body Problem," *Journal of Guidance, Control, and Dynamics* Vol. 30, No. 3, 2007, pp. 687-693. Doi: 10.2514/1.26232

[8] Heiligers, J., Ceriotti, M., McInnes, C. R., and Biggs, J. D. "Design of Optimal Transfers Between North and South Pole-Sitter Orbits," *22nd AAS/AIAA Space Flight Mechanics Meeting*. Charleston, SC, 2012.

[9] McInnes, C. R. *Solar Sailing: Technology, Dynamics and Mission Applications*. Berlin: Springer-Praxis Books in Astronautical Engineering, Springer-Verlag, 1999.

[10] Ceriotti, M., Heiligers, J., and McInnes, C. R. "Trajectory and Spacecraft Design for a Pole-Sitter Mission," *Journal of Spacecraft and Rockets*, 2012, Accepted subject to minor corrections. Doi:

[11] Becerra, V. M. "Solving Complex Optimal Control Problems at No Cost with PSOPT," *IEEE Multi-conference on Systems and Control*,Yokohama, Japan, 2010.

[12] Wächter, A., and Biegler, L. T. "On the Implementation of an Interior-point Filter Line-search Algorithm for Large-scale Nonlinear Programming," *Mathematical Programming* Vol. 106, No. 1, 2006, pp. 25-57. Doi: 10.1007/s10107-004-0559-y

[13] Gill, P. E., Murray, W., and Saunders, M. A. "SNOPT: An SQP Alghorithm for Large-Scale Constrained Optimization," *SIAM Journal on Optimization* Vol. 12, No. 4, 2002, pp. 979-1006. Doi: 10.1137/S1052623499350013

[14] Llanos, P. J., Hintz, G. R., Lo, M. W., and Miller, J. K. "Powered Heteroclinic, Homoclinic Connections between the Sun-Earth Triangular Points and Quasi-Satellite Orbits for Solar Observations," *2013 Astrodynamics Specialist Conference*. Hilton Head, South Carolina, USA, 2013.

[15] Turner, D. L., and Li, X. "Using spacecraft measurements ahead of Earth in the Parker spiral to improve terrestrial space weather forecasts," *Space Weather* Vol. 9, No. 1, 2011. Doi: 10.1029/2010SW000627